

On the mechanism of vertical stabilizer plates for improving aerodynamic stability of bridges

Airong Chen[†], Zhiyong Zhou[‡], and Haifan Xiang^{††}

State Key Laboratory for Disaster Reduction in Civil Engineering
Department of Bridge Engineering, Tongji University, Shanghai, China

(Received February 2, 2004, Accepted December 8, 2005)

Abstract. Vertical stabilizer plates have been found to be an effective aerodynamic measure to improve the aerodynamic stability of bridges either with an open cross section or with a streamlined box cross section in wind tunnel testings and have been adopted in some long span bridges. By taking an open deck II-shaped section and a closed box section as examples, the mechanism of vertical stabilizer plates for improving aerodynamic stability are investigated by using numerical simulation based on Random Vortex Method. It is found that vertical stabilizer plates can increase the amplitude of the heaving motion, and decrease that of the rotational motion of the bridge decks.

Keywords: bridge deck; aerodynamic stability; aerodynamic measure; vertical stabilizer plate; random vortex method (RVM).

1. Introduction

Geometrical shape of cross-sections of long span bridges is often chosen based on the consideration of aerodynamic stabilities. Proper aerodynamic measures to improve the aerodynamic stability of bridges are necessary if the aerodynamic stability of cross sections chosen can't meet the design criteria. Vertical stabilizer plates have been found to be an effective aerodynamic measure to improve the aerodynamic stability of bridges in wind tunnel testings. This kind of measure has been adopted in Akashi Kaikyo Bridge in Japan and in Runyang Bridge over Yangtze River in China (a suspension bridge with a main span of 1490 m).

The self-excited forces of bridge decks can be expressed by eight aerodynamic derivatives (Scanlan 1974) which can characterize the flutter instability and are still widely used nowadays. These aerodynamic derivatives are H^*_1 , H^*_2 , H^*_3 , and H^*_4 for unsteady heaving and A^*_1 , A^*_2 , A^*_3 , and A^*_4 for unsteady pitching motions. Broadly speaking, the flutters of bridges are primarily classified into two categories: the torsional flutter and the coupled flutter. In these eight aerodynamic derivatives, A^*_2 is the key one for flutter investigation. If A^*_2 shows positive, the bridge may exhibit torsional flutter, otherwise the coupled flutter may occur.

[†] Professor, Corresponding Author, E-mail: a.chen@mail.tongji.edu.cn

[‡] Associate Professor

^{††} Professor

While the flutter instabilities are characterized by these eight aerodynamic derivatives, it is difficult to control each aerodynamic derivative by changing the geometrical shape of bridge decks [Masaru Matsumoto, Hiromichi Shirato, etc, Flutter stabilization of long span bridges, The Second International Symposium on Wind and Structures, Busan, Korea (2002) 257-264 2002]. In other words, the relationship between the aerodynamic derivatives and the geometrical shape of bridge decks are highly complex and difficult to ascertain.

It is well known that two distinct features of unsteady separated flow about bluff bodies either stationary or in motion, are vortex shedding and vortex motion. The complicated vortex structures and development of vortex motion in the near wake directly influence the aerodynamic forces on the bluff bodies. As a consequence, we may identify the inherent mechanism of the fluid forces on the bodies by investigating the complicated vortex structure and motion.

Random Vortex Method (RVM) is a kind of discrete vortex methods, which are based on the particle discretization of the vorticity-velocity formulation of the Navier-Stokes equation in the Lagrangian form. They are grid-free, with little or no numerical diffusion and naturally adaptive. The discrete vortex methods have been generalized in many applications and can apply to complex high-Reynolds-number separated flow. Larsen and Walther (1997) have undertaken the pioneer work on the aeroelastic analysis of bridge decks based on the discrete vortex method.

To understand how the vertical stabilizer plates can improve the aerodynamic stability, the numerical simulation based on the RVM is employed (Zhou 2002). Two-dimensional viscous flow about a D-shaped section and a streamlined section are simulated. Four arrangements of vertical plates on the open cross section and vertical plates with different heights at the top of the streamlined deck are investigated.

2. The random discrete vortex method

In RVM, the boundary element method and the generalized Biot-Savart integral are used to determine effectively the surface vorticity about a group of isolated bodies (multi-bodies) in two-dimensional viscous incompressible flow. The solution to the unknown surface vorticity is made unique by imposing the principle of conservation of total vorticity all bodies as well as each single body. The vortex transport equation (VTE) is solved by two fractional step methods.

2.1. Governing equation

The two-dimensional incompressible unsteady flow of viscous fluid may be determined by the vorticity formulation of the Navier-Stokes equation:

$$\frac{\partial \omega(\mathbf{x}, t)}{\partial t} + (\mathbf{u}(\mathbf{x}, t) \cdot \nabla) \omega = \nu \nabla^2 \omega(\mathbf{x}, t) \quad (1a)$$

Where $\omega (\omega \equiv \nabla \times \mathbf{u})$ is the vorticity, $\mathbf{u}(\mathbf{x}, t)$ is the fluid velocity and ν denotes the kinematic viscosity.

The kinematic relationship between the velocity field and the vorticity field is obtained by solving the following Poisson equation:

$$\Delta \mathbf{u}(\mathbf{x}, t) = -\nabla \times \omega \quad (1b)$$

When the flow around solid configuration in motion, Eq. (1b) may be formulated as an integral

equation, the generalized Biot-Savart integral (Wu 1976):

$$\mathbf{u}(\mathbf{x}, t) = \mathbf{U}_\infty(t) - \frac{1}{2\pi} \iint_f \omega_f \times K(\mathbf{x}_f - \mathbf{x}) df + \frac{1}{2\pi} \oint_s \frac{(\mathbf{u}_s \cdot \mathbf{n}_s)(\mathbf{x}_s - \mathbf{x}) - (\mathbf{u}_s \times \mathbf{n}_s) \times (\mathbf{x}_s - \mathbf{x})}{|\mathbf{x}_s - \mathbf{x}|^2} dS \quad (1c)$$

With

$$K(\mathbf{x}_f - \mathbf{x}) = \frac{\mathbf{x}_f - \mathbf{x}}{|\mathbf{x}_f - \mathbf{x}|^2}$$

where $\mathbf{U}_\infty(t)$ is the freestream velocity, \mathbf{n}_s is the outward normal vector of the solid boundary, f is the fluid region and S is the solid boundary and $\mathbf{u}_s(\mathbf{x}_s, t)$ is the solid velocity on the surface(S) at \mathbf{x}_s .

At the solid boundary, the fluid velocity ($\mathbf{u}(\mathbf{x}_b, t)$) must be equal to the solid velocity ($\mathbf{u}(\mathbf{x}_s, t)$)

$$\mathbf{u}(\mathbf{x}_s, t) \cdot \mathbf{n}_S = \mathbf{u}_b(\mathbf{x}_b, t) \cdot \mathbf{n}_S; \quad \mathbf{u}(\mathbf{x}_s, t) \times \mathbf{n}_S = \mathbf{u}_b(\mathbf{x}_b, t) \times \mathbf{n}_S \text{ on } S \quad (1d)$$

With

$$\mathbf{u}_s(\mathbf{x}_b, t) = \mathbf{u}_h(\mathbf{x}_b, t) + \Omega(t) \mathbf{e}_z \times (\mathbf{x}_c(t) - \mathbf{x}_b(t))$$

where $\mathbf{u}_h(\mathbf{x}_b, t)$ is the vertical velocity of the solid, $\Omega(t)$ is the rotational angular velocity and \mathbf{x}_c is the center of mass.

At infinity we have

$$\mathbf{u}(\mathbf{x}, t) = \mathbf{U}_\infty(t) \text{ when } \mathbf{x} \rightarrow \infty \quad (1e)$$

In the discrete vortex methods, the vorticity field is considered as a discrete sum of the individual vorticity fields of the particles, having core radius σ , strength $\Gamma(t)$ and an individual distribution of vorticity determined by the function f_σ so that

$$\omega_f(\mathbf{x}, t) = \omega_\sigma(\mathbf{x}, t) = \sum_{i=1}^{N_V} \Gamma_i(t) f_\sigma(\mathbf{x} - \mathbf{x}_i) \quad (2)$$

Where N_V is total number of the vortex particle, which is described as vortex blob.

2.2. Determination of the vorticity boundary condition

The generalized Biot-Savart integral (Eq. (1c)) is valid for both the fluid domain (f) and the solid domain (B). Owing to the generation of the fluid vorticity in the boundary region, we introduce a fluid layer, S^+ adjacent to the solid surface, S . When the thickness of the fluid layer f_s extend to infinitesimal, it is convenient to introduce the surface vortex sheet γ_{S^+} . As a consequence, we have the following vector equation.

$$\mathbf{u}(\mathbf{x}, t) = \mathbf{U}_\infty(t) - \frac{1}{2\pi} \iint_f \omega_f \times K(\mathbf{x}_f - \mathbf{x}) df + \frac{1}{2\pi} \oint_s \frac{(\mathbf{u}_s \cdot \mathbf{n}_s)(\mathbf{x}_s - \mathbf{x}) - (\mathbf{u}_s \times \mathbf{n}_s) \times (\mathbf{x}_s - \mathbf{x})}{|\mathbf{x}_s - \mathbf{x}|^2} dS \quad (3)$$

According to Eq. (3), we have the following vector equation for each vortex sheet γ_{S^+} in discrete form

$$\sum_{j=1}^{N_s} \oint_{S_j} \frac{\gamma_{S^+} e_z \times (\mathbf{x}_{S^+} - \mathbf{x}_S)}{|\mathbf{x}_{S^+} - \mathbf{x}_S|^2} dS = \sum_{j=1}^{N_s} \left\{ \oint_{S_j} \frac{(\mathbf{u}_S \cdot \mathbf{n}_S)(\mathbf{x}_S - \mathbf{x}_{S^+}) - (\mathbf{u}_S \times \mathbf{n}_S) \times (\mathbf{x}_S - \mathbf{x}_{S^+})}{|\mathbf{x}_S - \mathbf{x}_{S^+}|^2} dS \right\} + \int_{f-S^+} \omega_f \times K(\mathbf{x}_f - \mathbf{x}_{S^+}) df + 2\pi[\mathbf{U}_\infty(t) - \mathbf{u}_S(\mathbf{x}_{S^+})] \quad (4)$$

where $\mathbf{u}_S(\mathbf{x}_{S^+})$ is the velocity on the boundary of the solids at \mathbf{x}_{S^+} . N_s is the number of the solids.

The normal and tangential components of the vector Eq. (4) are the first Fredholm integral equations in unknown γ_{S^+} and its solution is not unique according to the nature of Fredholm integral equation. The solution may be made unique by imposing a constraint based on the principle of the conservation of total vorticity. According to the principle, the total vorticity does not change with time (Wu 1976).

$$\partial \left(\int_f \omega df + \sum_j^{N_s} 2\Omega_j A_j \right) / \partial t = 0 \quad (5)$$

where Ω_j , A_j are the rotational angular velocity and the area of the j -th solid, respectively.

Using Eq. (2) in Eq. (5), in discrete form, the following equations can be obtained

$$\left\{ \sum_{i=1}^{N_v^k} \Gamma_i^k + \sum_{j=1}^{N_s} 2\Omega_j^k A_j + \sum_{j=1}^{N_s} \sum_{i=1}^{M_j} \gamma_{i,j}^k l_{i,j} \right\} - \left\{ \sum_{i=1}^{N_v^{k-1}} \Gamma_i^{k-1} + \sum_{j=1}^{N_s} 2\Omega_j^{k-1} A_j + \sum_{j=1}^{N_s} \sum_{i=1}^{M_j} \gamma_{i,j}^{k-1} l_{i,j} \right\} / \Delta t = 0 \Rightarrow$$

$$\sum_{j=1}^{N_s} \sum_{i=1}^{M_j} \gamma_{i,j}^k l_{i,j} = -\Gamma^{a,k-1} - 2 \sum_{j=1}^{N_s} (\Omega_j^k - \Omega_j^{k-1}) A_j \quad \text{with} \quad \Gamma^{a,k-1} = \sum_{i=1}^{N_v^k} \Gamma_i^k - \left\{ \sum_{i=1}^{N_v^{k-1}} \Gamma_i^{k-1} + \sum_{j=1}^{N_s} \sum_{i=1}^{M_j} \gamma_{i,j}^{k-1} l_{i,j} \right\} \quad (6)$$

where N_v^k is the total number of vortex blob during the k -th time step, Γ_i^k is the circulation of i -th vortex blob at k -th time step, $l_{i,j}$ is the length of the i -th boundary element on the j -th solid surface, M_j is the total number of boundary elements on the j -th solid and $\Gamma^{a,k-1}$ is the total circulation of vortex blobs that have entered bodies and have been removed from numerical calculation during the $(k-1)$ -th time step.

The principle of the conservation of the total vorticity is applied to each body, as a consequence, the following equations can be obtained

$$\sum_{i=1}^{M_j} \gamma_{i,j}^k l_{i,j} = -\Gamma_j^{a,k-1} - 2(\Omega_j^k - \Omega_j^{k-1}) A_j \quad j=1, 2, \dots, N_s \quad (7)$$

where $\Gamma_j^{a,k-1}$ is total circulation of the vortex blobs entered j -th solid during the $(k-1)$ -th time step.

In this paper, the normal component of Eq. (4), Eq. (6) and Eq. (7) are solved by applying the least square method (Walther 1997 and Wu 1976).

2.3. Computation of convection, diffusion equation and aerodynamic force

In RVM, the VTE may be solved by two fractional steps method (Chorin 1973), in a Lagrangian formulation. Firstly, we solve the convection equation with $d\Gamma_i/dt = 0 (I = 1, \dots, N_v)$ by standard ODE method. In this paper, we use the Euler method. Secondly, we approximated the diffusion equation by random walks method developed by Chorin (1973). As a consequence, the solution to VTE using the Heun integration method is

$$\mathbf{x}_i^{k+1} = \mathbf{x}_i^k + \frac{1}{2} \mathbf{u}_i^k \Delta t + \eta_i \quad (8)$$

where Δt is the time step, η_i are random vector with zero mean and variance $2\nu\Delta t$.

The costly $O(N_v^2)$ operation imposed by solving the Eq. (8) can be overcome by applying the $O(N_v)$ fast adaptive multipole algorithm developed by Carrier (1988).

Applying the moment of momentum on the boundary of bluff bodies, introducing body-fitting coordinate and combining vorticity transport equation, then we have the following equation in the discrete form:

$$\left(\frac{\partial p}{\partial s}\right)_{i,j}^k = -\frac{\gamma_{i,j}^k - \gamma_{i,j}^{a,k-1} l_{i,j}}{\Delta t} - \mathbf{a}_{i,j}^k \quad (9)$$

where $\mathbf{a}_{i,j}^k$ is the tangential acceleration on the midpoint of the i -th boundary element of the j -th body. Aerodynamic forces may be obtained by the integration of pressure distribution along the boundary of the bodies. It must be noted that the aerodynamic forces obtained by Eq. (9) is only the force components due to pressure distribution along the surface of bodies and exclude the viscous shear at the surface.

The self-excited force per unit span may be expressed as

$$F_{L,e} = (1/2)\rho U^2 2B(KH_1^* \dot{h}/U + KH_2^*(B\dot{\alpha})/U + K^2 H_3^* \alpha + K^2 H_4^* h/B) \quad (10a)$$

$$F_{M,e} = (1/2)\rho U^2 2B^2(KA_1^* \dot{h}/U + KA_2^*(B\dot{\alpha})/U + K^2 A_3^* \alpha + K^2 A_4^* h/B) \quad (10b)$$

Where $K(K = U/(fB))$ is reduced frequency, h , α , \dot{h} , $\dot{\alpha}$ are vertical motion, rotational motion and their first derivatives, respectively, A_i^* , $H_i^* (i = 1, 2, 3, 4)$ are aerodynamic derivatives

In order to compute the aerodynamic derivatives, the following procedure may be applied: Firstly, the lift and moment time traces of bridge deck oscillated in either pure vertical and rotational motion are computed by RVM; Secondly, the aerodynamic derivatives may be identified from the bridge deck motion and aerodynamic forces by a least square fitting of a sinusoid to the simulated lift and moment time traces (Larsen 1997).

3. Aerodynamic stability of Π -shaped section with stabilizers

The prototype cross section of Jinsha Bridge over Yangtze River, a concrete cable-stayed bridge with a main span of 500 m, is shown and four arrangements of vertical plate vertical to the cross section are presented in Fig. 1, which are denoted as B type section, C type section, D type section and E type section, respectively, and the height of vertical plates all are 1.9 m.

Fig. 2(a) illustrates that a 'vortex B' is being generated at the lower windward corner of the

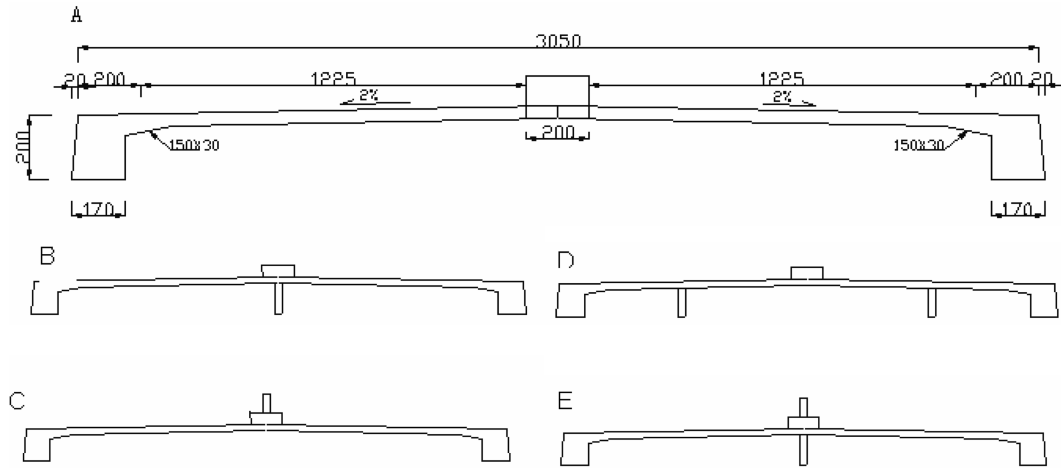


Fig. 1 Geometry of a bridge deck with an open cross section

bridge deck and a 'vortex A' is convecting downstream across the under side of the prototype deck at the non-dimensional time $t_1 = Ut/B = 5.64$ (where $B =$ width of deck). The 'vortex A' cause a higher local suction pressure at the local location $x_1/B = 0.21$. The higher local suction pressure is acting in an opposite direction against the body motion such that the value of work done by the suction pressure is negative within a non-dimensional time interval $U\Delta t/B = 0.02$ as indicated in Fig. 4.

At the instants $t_2 = 6.06$, the 'vortex B' is strengthened and its scale becomes larger and the 'vortex A' has reached the right leeward corner resulting in the maximum of lift force and moment. The value of work done by the suction pressure induced by the 'vortex A' is positive and the value by 'vortex B' is negative. As the width of the local suction pressure induced by the 'vortex A' is shorter than it by 'vortex B', the work done by the suction pressure induced by the vortex on the lower bridge deck is negative as indicated in Fig. 4.

Fig. 2(c) and Fig. 2(d) illustrate that the 'vortex A' has entered the near wake. As can be seen, the flow pattern at the instants $t_4 = 6.6$ is almost the same as that of Fig. 2(c) but the direction of the body motion has reversed resulting in a positive work done by the suction pressure as indicated in Fig. 4.

Fig. 2(e) illustrates that the 'vortex B' is convecting downstream across the under side of the bridge deck at the instants $t_5 = 7.5$ and begins to repeat the flow process undergone by 'vortex A'. At the same time, a new 'vortex C' is being generated at the lower windward corner and begins to repeat the flow process undergone by 'vortex B' (compare with Fig. 2b). At the instants t_2 and t_6 or t_1 and t_5 the similarity of vortex structure explains the aerodynamic behavior of the deck as indicated in Fig. 2 and Fig. 3.

Fig. 5 illustrates the aerodynamic derivatives obtained by means of RVM simulations and wind tunnel test results for flow about the prototype section. A comparison of prototype critical wind speeds obtained from the RVM simulations and from wind tunnel section model tests is given in Table 1. Fig. 5 and Table 1 show the aerodynamic derivatives, in particular, A_2^* and the computed critical wind speed for the onset of flutter is in good agreement with the wind tunnel results. Moreover Fig. 5 illustrates that the A_2^* shows positive at the non-dimensional wind velocity $U/fB = 5.5$, so the torsional flutter can be excited.

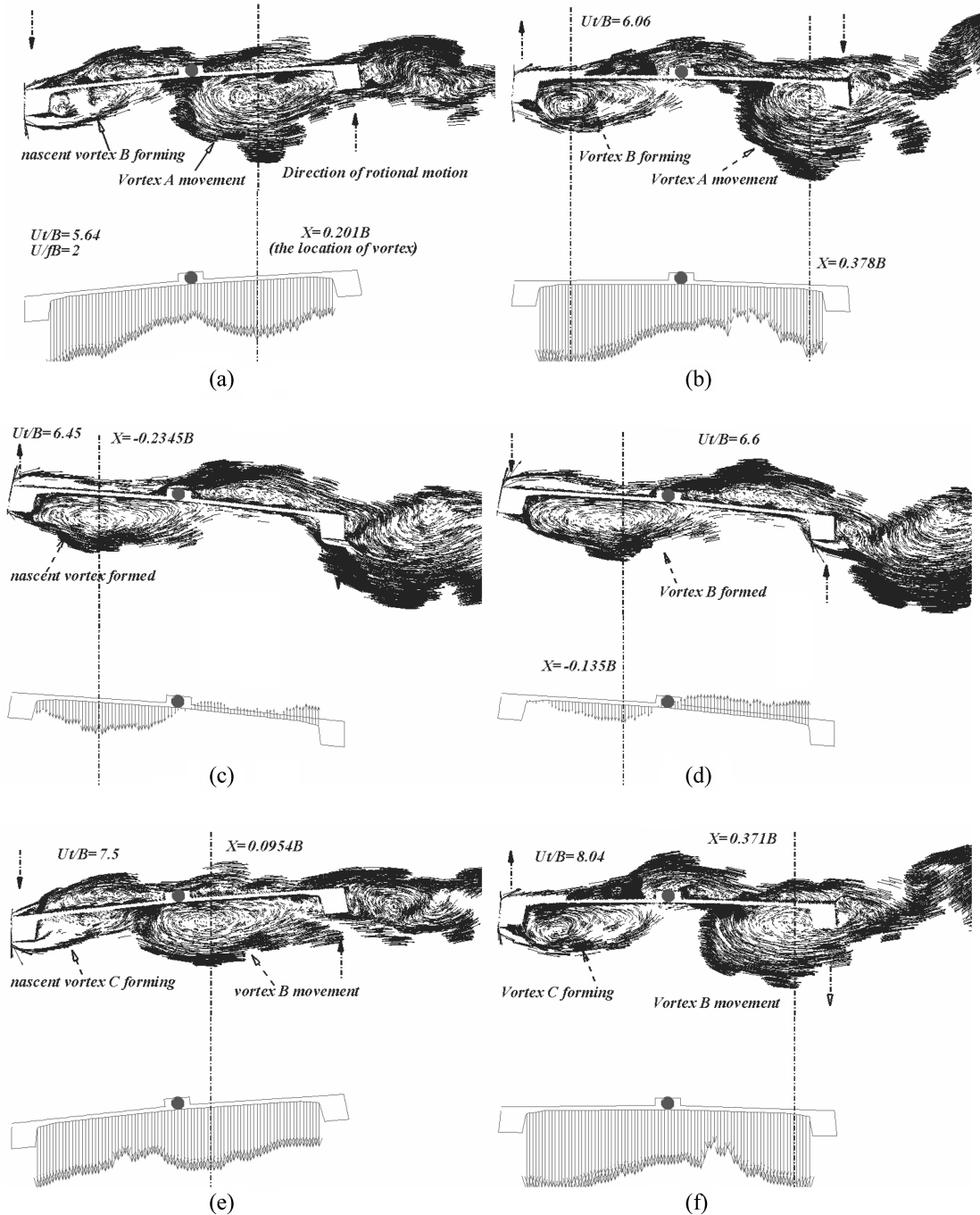


Fig. 2 Instant flow pattern for flow about the prototype section (the non-dimensional wind velocity $U/fB = 2$)

From the above interpretation of Fig. 2 it can be concluded that the separation bubble generates at the lower windward corner and the main vortex structure developed from the separation bubble

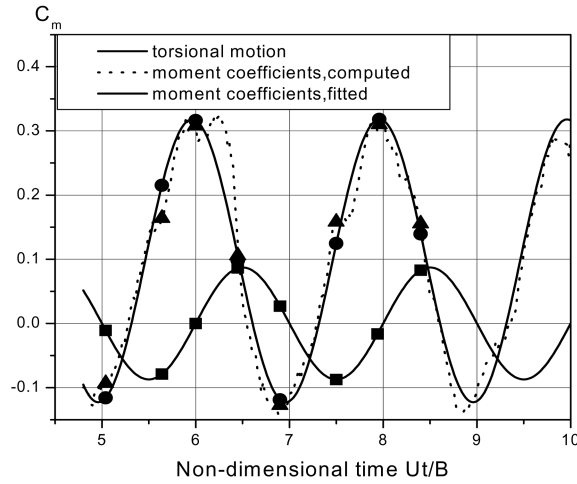


Fig. 3 Rotational motion and computed and fitted time traces of moment for flow about the prototype deck ($U/fB = 2$) (W_v is the work done by the suction pressure between the non-dimensional interval 0.02)

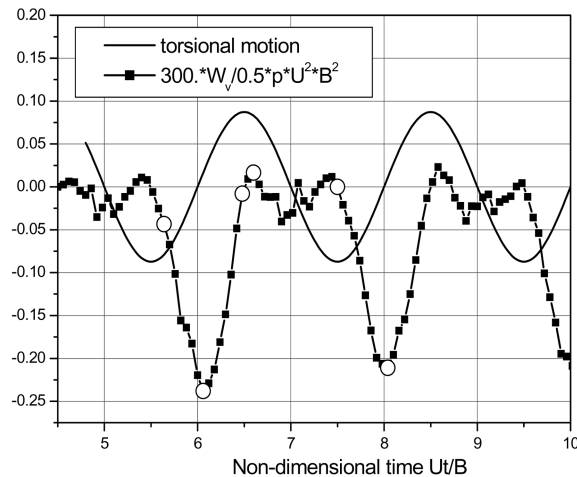


Fig. 4 Rotational motion and computed time traces of power done by the vortex generated at the lower windward corner and convected across the under side for flow about the prototype cross-section ($U/fB = 2$)

convects across the under side of the bridge deck downstream into the wake. The value of the work done by the local suction pressure induced by the vortices is determined by the unsteady interaction effect of the local suction pressure and the body motion. The period of vortex shedding at the lower windward corner and the development of vortex motion around the under side of the prototype bridge deck make a direct influence on the value of the work done.

Based on the above observation, a B-type section and a C-type section with a vertical plate at the mid-chord point and two vertical plates at the soffit of the bridges are proposed as aerodynamics measures to improve flutter stability (see Fig. 1), also D-type section and E-type section are proposed as reference sections. It is our aim to attempt to weaken the strength of the main vortex structure developed from the separation bubble and destroy its rhythmic motion.

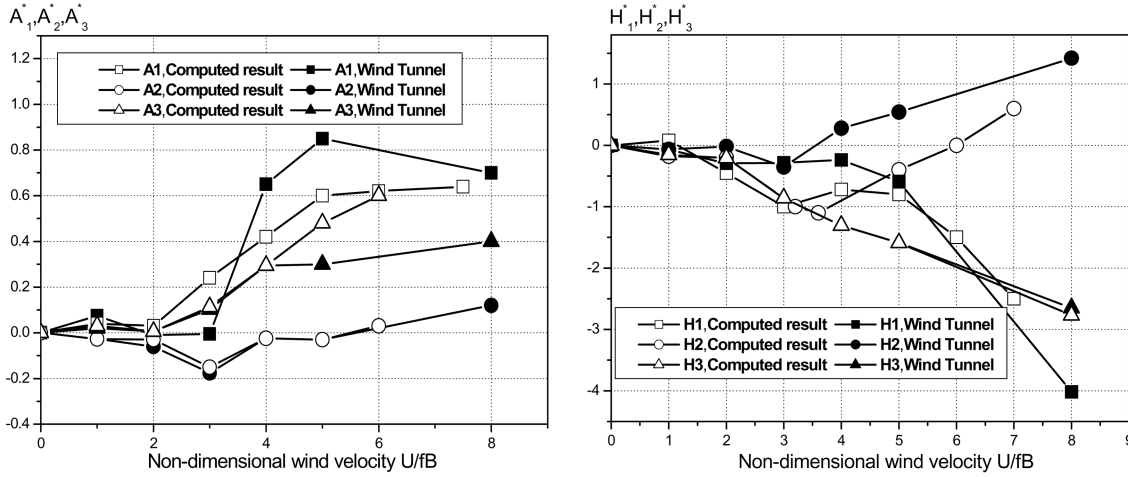


Fig. 5 Aerodynamic derivatives for prototype cross-section

Table 1 Structural parameters critical wind speed for the onset of flutter for prototype section (wind incidence 0 degree)

B (m)	M (Kg/m)	I (Kgm)	f_h (Hz)	f_α (Hz)	Critical wind speed (m/s)	
					Present work	Wind tunnel testing
27	44,300	4,260,000	0.2801	0.4540	62 ($\xi=0$)	58 ($\xi=0$)
					83 ($\xi=0.01$)	88 ($\xi=0.01$)

Note: B : deck width; M : mass per unit length; I : mass inertia moment; f_h : vertical bending frequency; f_α : torsional frequency; ξ : structure damping (rel-to-crit)

RVM simulations were carried out for the following four bridge cross-sections following the procedure outlined above. The simulations covered the reduced wind speed range $1 < U/fB < 10$. Bending simulations were carried out at a forced motion amplitude $h/B = 0.05$. Twisting simulations were carried out at $\alpha = 5^\circ$. Fig. 6a and Fig. 6b illustrate the flow pattern for flow about prototype deck and D-type section at $U/fB = 6$ and Fig. 7 illustrates the rotational motion and computed and fitted time traces of moment for flow about prototype section and D-type section at $U/fB = 6$, respectively. Fig. 8 illustrates the rotational motion and computed time traces of power done by the vortex generated at the lower windward corner and convected across the under side for flow about prototype section and D-type section at $U/fB = 6$, respectively.

Aerodynamic derivatives obtained for the five generic sections presented are shown in Fig. 9.

Fig. 9 illustrates the aerodynamic derivative A_2^* are positive at reduced wind velocity (U/fB) = 7 for the C-type section, so the torsional flutter can be excited and the C-type arrangement of vertical plates can not change the torsional flutter pattern from the prototype section. It is also shown from Fig. 9 that the aerodynamic derivative A_2^* is negative for B-type, D-type and E-type sections, and the coupled flutter may still occur. So it can be concluded that the characteristics of flutter can be changed to from “torsional” to “coupled” by arranging the vertical plates at the soffit of the prototype section.

The work done in one oscillation cycle by the suction pressure induced by the vortex for the prototype deck cross-section, B-type cross-section, C-type cross-section, D-type cross-section and E-

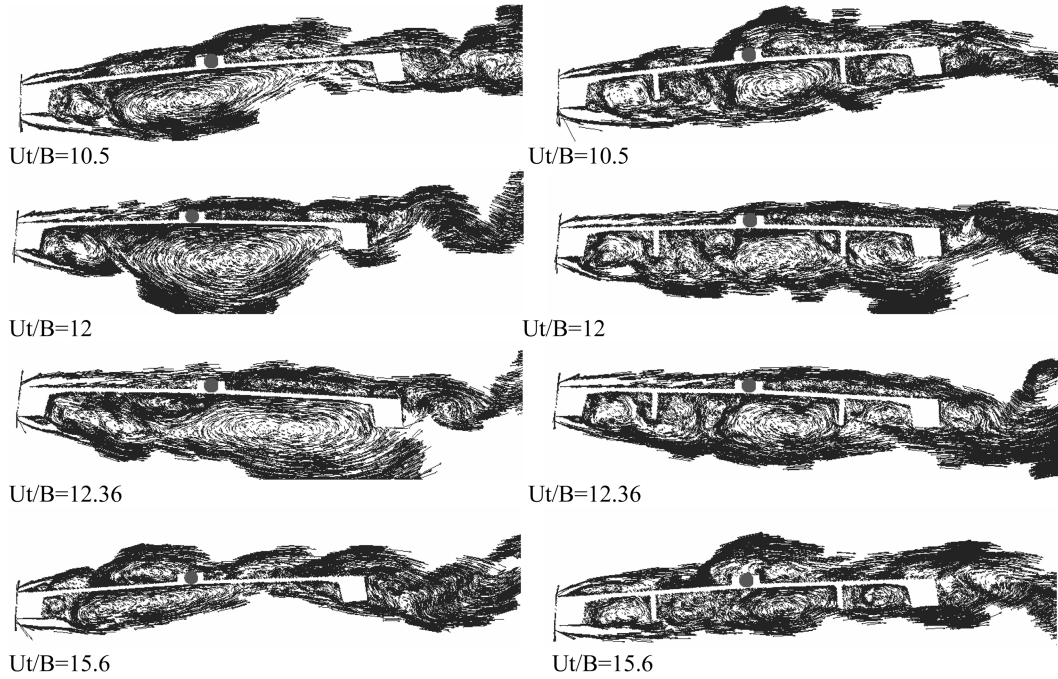


Fig. 6 Instant flow pattern for flow about the prototype section and D-type section at $U/B = 6$

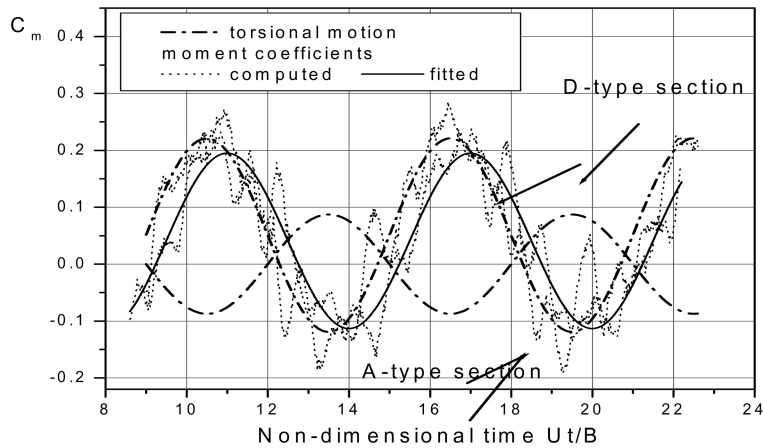


Fig. 7 Rotational motion and computed and fitted time traces of moment for flow about prototype section and D-type section at $U/B = 6$, respectively

type cross-section, respectively, are given in Table 2.

Table 3 shows the computed critical wind speed for the onset of flutter for A-type, B-type, C-type, D-type and E-type sections, respectively. It can be seen from Table 2 and Table 3 that the value of the work done in one oscillation cycle by the vortices for the prototype deck is positive and the value of the work for B-type, C-type, D-type and E-type sections is negative. It can be concluded that the critical wind speed for the onset of flutter can be increased if the vertical plate is

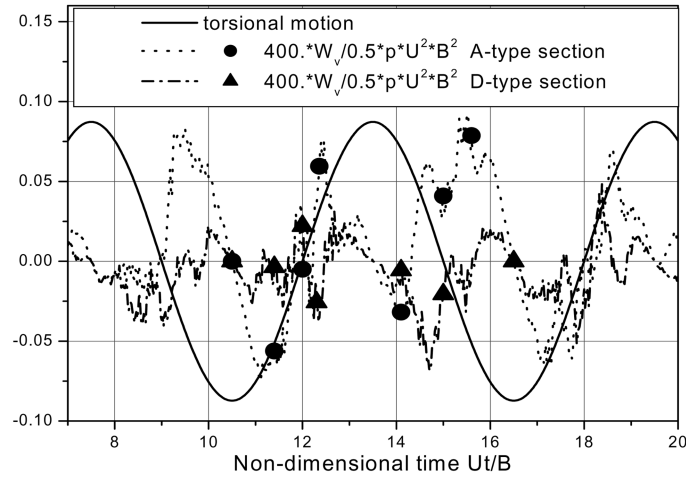


Fig. 8 Rotational motion and computed time traces of power done by the vortex generated at the lower windward corner and advected around the lower side for flow about prototype section and D-type section at $U/fB = 6$, respectively

Table 2 Work done in one oscillation cycle by the suction pressure induced by the vortices at the soffit of the bridge deck for the prototype deck cross-section, B-type cross-section, C-type cross-section, D-type cross-section and E-type cross-section, respectively

Section Type	A	B	C	D	E
$U/fB = 2$	-3.03E-2	-3.00E-2	-3.03E-2	-3.96E-2	-2.85E-2
$U/fB = 4$	-7.58 E-3	-2.58E-2	-1.65E-2	-2.09E-2	-2.37E-2
$U/fB = 6$	1.E-3	-7.50 E-3	-5.20 E-3	-1.03 E-2	-9.70E-3

Table 3 Critical wind speeds for the onset of flutter for A, B, C, D and E-type sections (structure damping is 0)

Section Type	A	B	C	D	E
Critical wind speed (m/s)	62	86	97	123	129

attached at the soffit of the prototype section and the flutter mode is changed from the torsional flutter into the coupled flutter and the critical wind speed for the onset of flutter can also be increased if the vertical plate is located at the top center of the prototype section, however, the flutter mode remains as the torsional flutter instead of the coupled flutter.

4. Aerodynamic stability of streamlined box with stabilizers

Runyang Bridge over Yangtze River is a suspension bridge with a main span of 1490 m and a closed box deck of only 3 m high (Fig. 10). A series of wind tunnel testings have been carried out at the State Key Laboratory for Disaster Reduction in Civil Engineering at Tongji University. It was found that the original design could not meet the design criteria, therefore, the vertical stabilizer plate of 0.8 m high was proposed at the center top of the box girder to improve the aerodynamic stability. To understand the mechanism, numerical simulations for the deck with and without

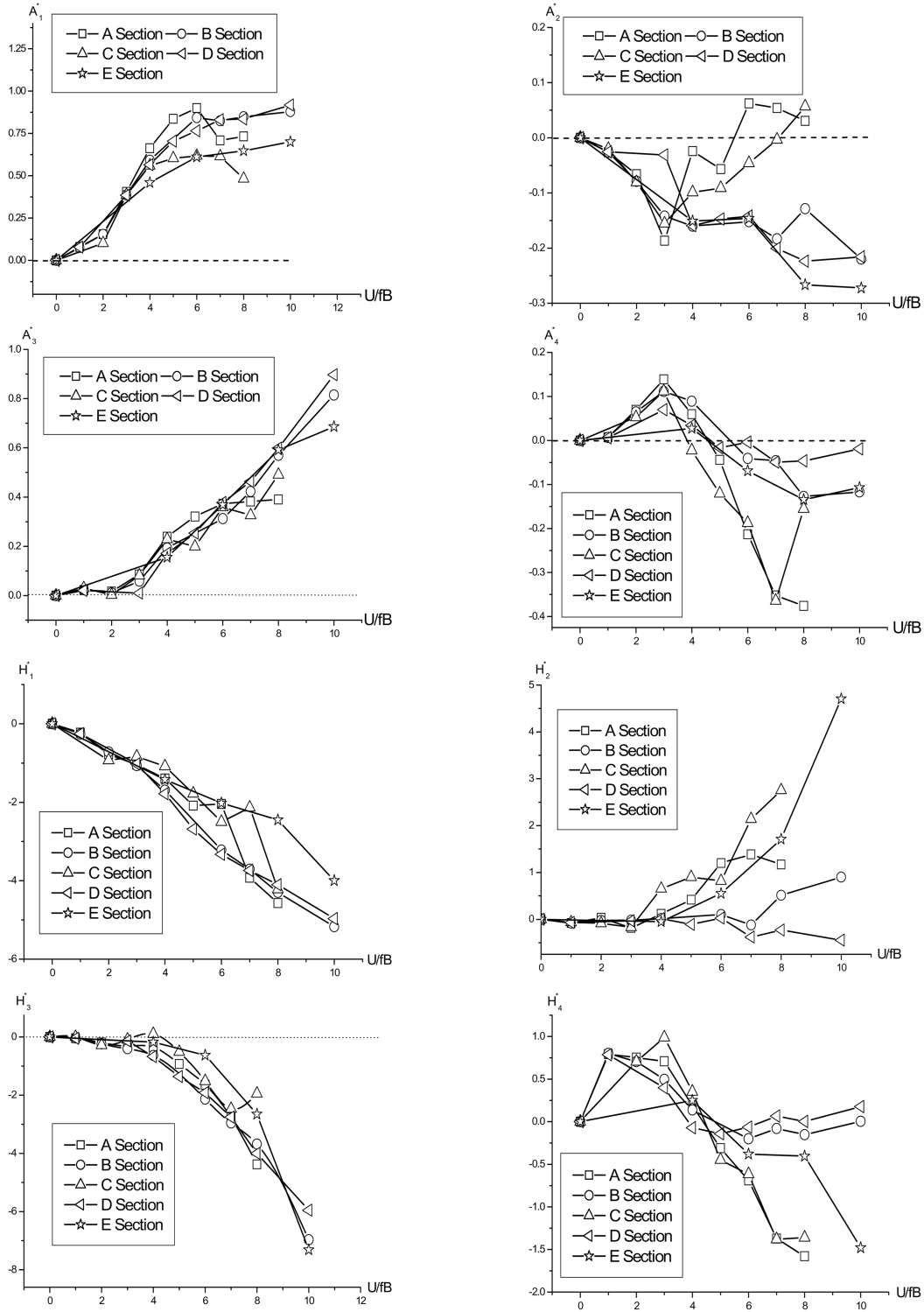


Fig. 9 Aerodynamic derivatives for the open cross-section of Jinsha Bridge with stabilizer plates

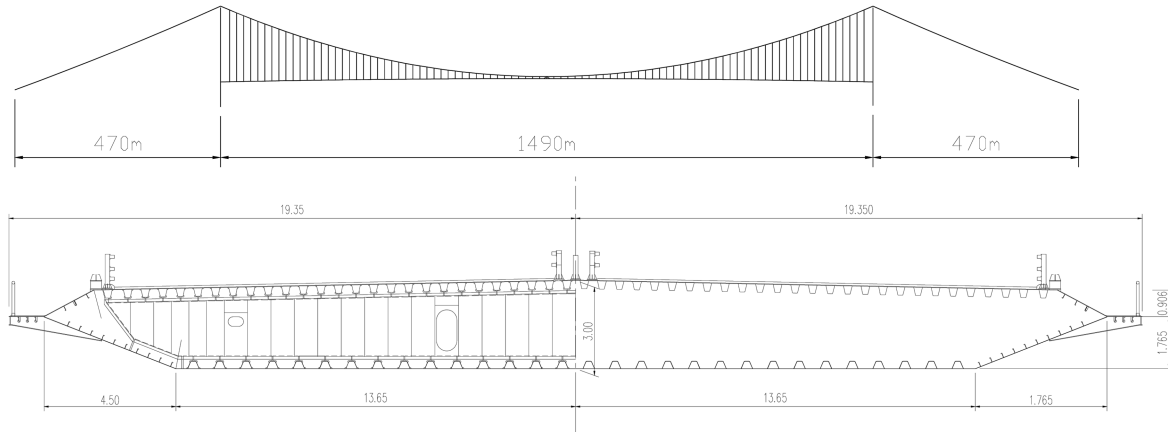


Fig. 10 Structural scheme of Runyang Bridge

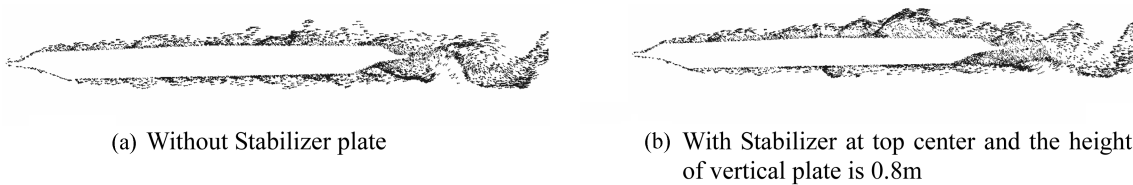


Fig. 11 Simulated flow pattern for Runyang Bridge in rotational motion at $U/fB = 8$ and $U/B = 12.5$. (the height of vertical plate is 0 m and 0.8 m respectively)

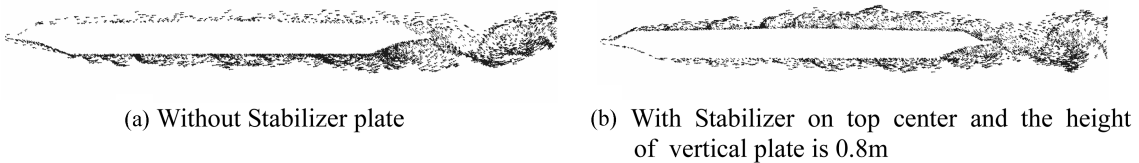


Fig. 12 Simulated flow pattern for Runyang Bridge in heaving motion at $U/fB = 8$ and $U/B = 12.5$

Table 4 Structural parameters of Runyang Bridge

B (m)	M (Kg/m)	I (Kgm)	f_h (Hz)	f_α (Hz)
38.7	30630	6642000	0.12426	0.23079

Table 5 Critical wind speeds for the onset of flutter or Runyang Bridge with vertical plates (wind attack angle 0 degree)

Height of vertical stabilizer plate (m)	0	0.5	0.65	0.8
Flutter speed (m/s) (Structure damping $\xi = 0.005$)	66.5	70.8	70.	75.
Flutter frequency (Hz)	0.2037	0.1988	0.2013	0.1935
Tested result of critical flutter velocity (m/s)	64.3	/	73.6	/

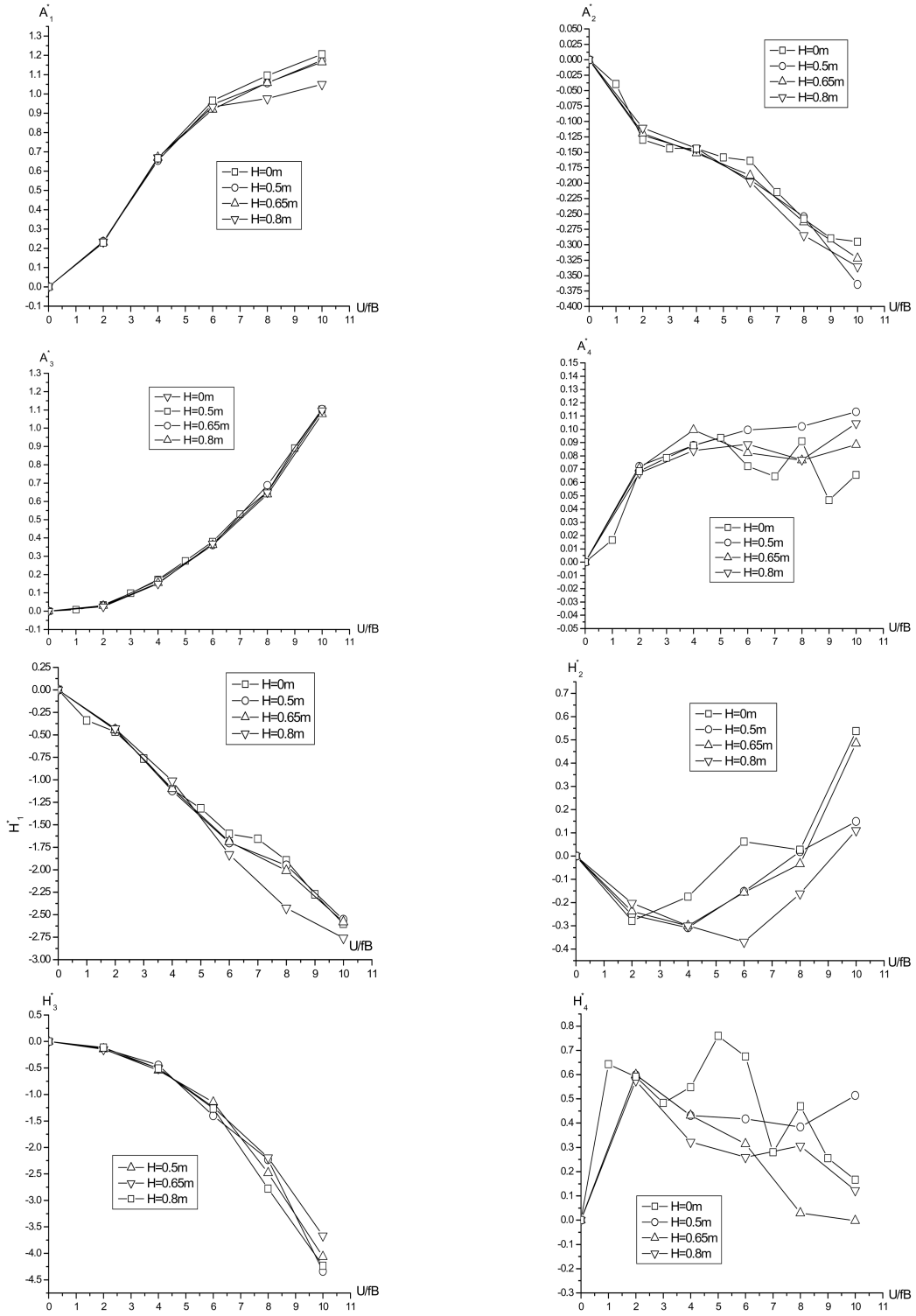


Fig. 13 Aerodynamic derivatives of Runyang Bridge with vertical plates of different heights

stabilizer plates were performed based on RVM method.

Fig. 11 and Fig. 12 respectively show the flow patterns of the deck in rotational and heaving motions without and with the stabilizer plate respectively. Fig. 13 shows the aerodynamic derivatives. Table 4 gives the basic parameters of the bridge, and Table 5 shows the critical flutter wind speeds of the bridge with vertical plates of different height.

The work done in two oscillation cycles for the deck without and with the center stabilizer plates in heaving and rotational motions are given in Table 6. It can be seen that the stabilizer plate increase the work done in heaving motion, whereas, the work done in rotational motion changes

Table 6 Work done in two oscillation cycles for the deck without and with the center stabilizer plates in heaving and rotational motions

Motion	Without stabilizer	With stabilizer of 0.8 m
Heaving	0.0497	0.0673
Rotational	0.3527	-0.0295

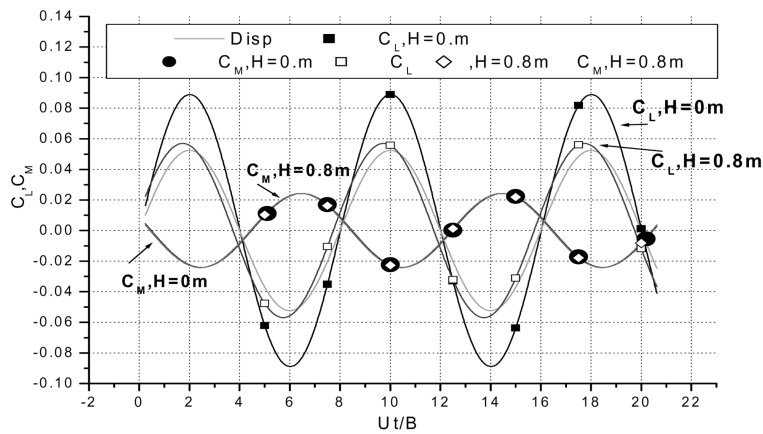


Fig. 14 Aerodynamic force coefficients of the deck in rotational motion at $U/fB = 8$

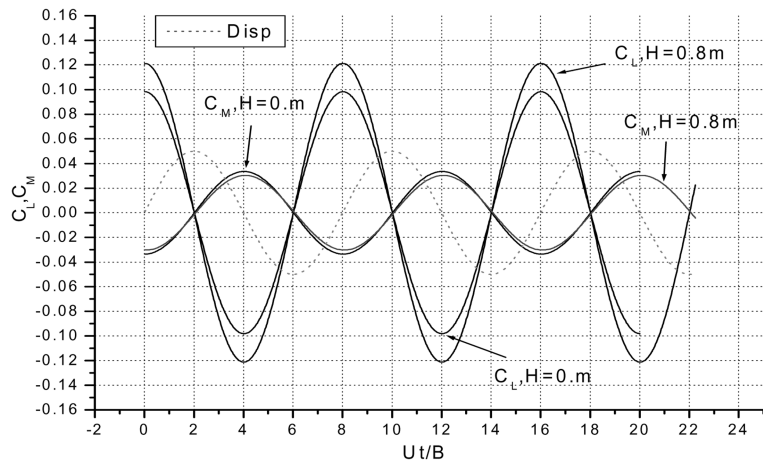


Fig. 15 Aerodynamic forces coefficients of the deck in heaving motion at $U/fB = 8$

from positive to negative. From Fig. 14 and Fig. 15, which show the aerodynamic force coefficients in rotational motion and heaving motion respectively, it is quite clear that due to the stabilizer the pitching moment decreases in rotational motion, and the lift increases in heaving motion.

5. Conclusions

From wind tunnel testings, it was found that the stabilizer plates are effective to improve the aerodynamic stability of bridges. To understand the mechanism, two-dimensional viscous flow about an open Π -shaped section and a streamlined closed box section are simulated based on the Random Vortex Method. The simulation results reveal that the separation bubble generates at the lower windward corner and the main vortex structure developed from the separation bubble convects downstream across the under side of the cross-section downstream into the wake. The value of the work done by the vortices is determined by the unsteady interaction effect of the local suction pressure and the body motion. The period of vortex shedding at the lower windward corner and the development of vortex motion across the under side of the prototype bridge deck make a direct influence on the value of the work. It can be concluded the critical wind speed for the onset of flutter may be increased when the strength of the main vortex structure is weakened and its rhythmic motion is destroyed. It can be seen that the critical wind speed for the onset of flutter can be largely increased if the vertical plate is attached at the soffit of the Π -shaped section, and the flutter characteristics can be changed from “torsional” to “coupled”. The critical wind speed for the onset of flutter can also be increased if the vertical plate is attached at the top center of the open cross section deck, however the flutter mode remains as “torsional”. The stabilizer plate attached at the top center of a closed box girder is also effective in increasing the critical flutter wind speed.

Acknowledgements

This research was jointly supported by the National Science Foundation of China under Grant No. 59895410 and the Excellent Teacher Program of the Education of Ministry of China.

References

- Belveau, J.G., Budlong, K.S., and Scanlan, R.H. (1974), “Indicial aerodynamic functions for bridge decks”, *J. Eng. Mech. Div., Proceeding of ASCE*, **100** (EM4).
- Carrier, J., Greengard, L., and Rokhlin, V. (1988), “A fast adaptive multiple algorithm for particle simulations”, *SIAM J. Sci. Statist. Comput.*, **9**(4), 669.
- Chorin, A. J. (1973), “Numerical study of slightly viscous flow”, *J. Fluid. Mech.*, 337-347.
- Larsen, Allan, Walther, Jens, H. (1997), “Aeroelastic analysis of girder sections based on discrete vortex simulations”, *J. Wind Eng. Ind. Aerodyn.*, **67&68**, 253-265.
- Matsumoto, Masaru and Shirato, Hiromichi etc., (2002), “Flutter stabilization of long span bridges”, *The second International Symposium on Wind and Structures*, Busan, Korea, 257-264.
- Walther, Jens, H., Larsen Allan (1997), “Two dimensional discrete vortex method for application to bluff aerodynamics”, *J. Wind Eng. Ind. Aerodyn.*, **67&68**, 183-193.
- Wu, J.C. (1976), “Numerical boundary conditions for viscous flow problems”, *AIAA*, **14**(8), 1042-1051.
- Zhou, Zhiyong, Chen, Airong, and Xiang, Haifang (2002), “Numerical assessment of aerodynamic derivatives and critical wind speed of flutter of bridge decks by discrete vortex method”, *J. Vib. Eng.*, **15**(3), 327-331 (in Chinese).